SAND2022-1881C

Transmitter Selection for Improved Information Gathering in Aerial Vehicle Navigation with Terrestrial Signals of Opportunity

Alexander A. Nguyen and Zaher M. Kassas
University of California, Irvine, USA

BIOGRAPHIES

Alexander A. Nguyen is a Ph.D. student in the Department of Mechanical and Aerospace Engineering at the University of California, Irvine and a member of the Autonomous Systems Perception, Intelligence, and Navigation (ASPIN) Laboratory. He received a B.S. in Mechanical Engineering with Honors from the University of California, Santa Barbara. His current research interests include motion planning, estimation theory, collaborative opportunistic navigation, and data association.

Zaher (Zak) M. Kassas is an associate professor at the University of California, Irvine and director of the Autonomous Systems Perception, Intelligence, and Navigation (ASPIN) Laboratory. He is also director of the U.S. Department of Transportation Center: CARMEN (Center for Automated Vehicle Research with Multimodal AssurEd Navigation), focusing on navigation resiliency and security of highly automated transportation systems. He received a B.E. in Electrical Engineering from the Lebanese American University, an M.S. in Electrical and Computer Engineering from The Ohio State University, and an M.S.E. in Aerospace Engineering and a Ph.D. in Electrical and Computer Engineering from The University of Texas at Austin. He is a recipient of the 2018 National Science Foundation (NSF) Faculty Early Career Development Program (CAREER) award, 2019 Office of Naval Research (ONR) Young Investigator Program (YIP) award, 2022 Air Force Office of Scientific Research (AFOSR) YIP award, 2018 IEEE Walter Fried Award, 2018 Institute of Navigation (ION) Samuel Burka Award, and 2019 ION Col. Thomas Thurlow Award. His research interests include cyber-physical systems, estimation theory, navigation systems, autonomous vehicles, and intelligent transportation systems.

ABSTRACT

A computationally efficient algorithm for selecting the most informative subset of terrestrial signals of opportunity (SOPs) is proposed. The following problem is considered. An aerial vehicle navigates in an environment where global navigation satellite system (GNSS) signals are unavailable. The aerial vehicle is equipped with an on-board receiver that extracts pseudorange observations from an abundant number of M terrestrial SOPs with known locations but unknown dynamic, stochastic clock error states (bias and drift). An extended Kalman filter (EKF) is employed to fuse these pseudorange observations to estimate the aerial vehicle's states (position and velocity) and the difference between the aerial vehicle-mounted receiver's clock error states and the clock errors of all SOPs. Due to size, weight, power, and cost (SWaP-C) constraints, the aerial vehicle should select a subset $K < M$ of the available SOPs with which it navigates. Since solving the optimal selection problem is rather involved, a sub-optimal, yet computationally efficient algorithm, termed opportunistic greedy selection (OGS), is proposed. The OGS is formulated by exploiting the additive, iterative properties of the Fisher Information Matrix (FIM), to minimize the aerial vehicle's average position error variance (i.e., A-optimality criterion). Numerical simulations are presented showing that the proposed OGS algorithm performs comparably with the optimal M choose K selection algorithm, but executes in a small fraction of the time. Furthermore, experimental results are presented for a U.S. Air Force high-altitude aircraft navigating without GNSS signals in an environment comprising $M = 57$ cellular terrestrial SOPs for 9.39 km in 105 s. It is shown that upon choosing $K = 15$ SOPs according to the proposed OGS algorithm, the position and velocity root mean square errors (RMSEs) were 11.45 m and 0.80 m/s, respectively. Monte Carlo results are presented arguing that the results achieved from the proposed OGS algorithm are very close to what the global optimal selection algorithm would yield.

I. INTRODUCTION

Modern aerial vehicle navigation systems, whether low altitude unmanned aerial vehicles (UAVs) or high altitude aircraft, heavily rely on global navigation satellite system (GNSS) signals [1]. However, relying on GNSS alone does not yield a continuous flow of reliable position, speed, and time estimates [2]. In recent years, GNSS radio frequency interference (RFI) events have increased dramatically, threatening the safety of flight operations [3] and calling for a reliable alternative to GNSS signals in the event that these signals become unusable [4].

Signals of opportunity (SOPs) [5,6] have been considered to enable navigation whenever GNSS signals become unusable. SOPs

Preprint of the 2022 ION ITM Conference
Long Beach, CA, January 25 – 27, 2022

can be terrestrial (e.g., AM/FM radio [7, 8], cellular [9–16], WiFi [17, 18], and digital television [19, 20],) or space-based (e.g., low Earth orbit (LEO) satellites [21–25]). These signals were not intended for navigation purposes but the literature has shown that they can be exploited for such purposes. SOPs are abundant, transmitted in a wide range of frequencies, more powerful than GNSS signals, and geometrically diverse. These inherent attributes of SOPs compensate for the limitations of GNSS signals. Nevertheless, the SOP states (position, velocity, and clock errors) are typically unknown during navigation, which requires them (or a subset of them) to be estimated on-the-fly in a process referred to as radio simultaneous localization and mapping (radio SLAM) [26]. Radio SLAM is analogous to the SLAM problem in the robotics literature [27].

This paper considers the following problem. An aerial vehicle is flying in an environment where GNSS signals are unavailable. The environment contains an abundant number of M terrestrial SOPs with known locations but unknown dynamic, stochastic clock error states (bias and drift). The aerial vehicle is assumed to be equipped with an on-board receiver capable of extracting pseudorange observations from the ambient SOPs' signals. An extended Kalman filter (EKF) is employed to fuse these pseudorange observations to estimate the aerial vehicle's states (position and velocity) and the difference between the aerial vehicle-mounted receiver's clock error states and the clock errors of all SOPs. Due to hardware and software limitations, the aerial vehicle is tasked with selecting a subset $K < M$ of the available terrestrial SOPs with which it navigates. Similar problems have been studied context of sensor and satellite selection. Past literature has shown that the sensor selection problem can be cast as a convex optimization problem [28–30] or piece-wise convex optimization problem [31, 32], which aim to select the optimal sensors with respect to a specific criterion. Furthermore, this problem has also been considered as a greedy sensor selection problem leveraging submodularity [33, 34], as well as a sensor selection problem based on exploiting the Fisher information matrix (FIM) [35–38]. It is worth pointing out that the sensor selection problems in the literature typically assume vehicle navigation via sensor fusion occurring over limited regions (on the order of tens to hundreds of meters). In contrast, this paper considers aerial vehicle navigation via signal fusion over a large region (on the order of tens to hundreds of kilometers). This paper found that the selected transmitters are still valid for an aircraft trajectory on the order of several kilometers, since the SOP geometry with respect to the aircraft are by and large stationary (for sufficiently faraway SOPs). A similar problem has also been considered in the context of satellite selection, in which the optimal GNSS satellite selection algorithms focused on the geometric dilution of precision (GDOP) metric [39, 40]. While these algorithms aimed to choose the satellites with the most favorable spatial distribution via the GDOP metric, this paper aims to maximize the information content from SOP pseudoranges by utilizing the FIM.

Since solving the optimal selection problem is rather involved, this paper proposes a sub-optimal, yet computationally efficient algorithm, termed opportunistic greedy selection (OGS). The OGS is formulated by exploiting the additive, iterative properties of the FIM, to minimize the aerial vehicle's average position error variance (i.e., A-optimality criterion). Numerical simulations are presented showing that the proposed OGS algorithm performs comparably with the optimal M choose K selection algorithm, but executes in a small fraction of the time. Furthermore, experimental results are presented for a U.S. Air Force high-altitude aircraft navigating without GNSS signals in an environment comprising $M = 57$ cellular terrestrial SOPs for 9.39 km in 105 s. It is shown that upon choosing $K = 15$ SOPs according to the proposed OGS algorithm, the position and velocity root mean square errors (RMSEs) were 11.45 m and 0.80 m/s, respectively. Monte Carlo results are presented arguing that the results achieved from the proposed OGS algorithm are very close to what the global optimal selection algorithm would yield.

The remainder of this paper is organized as follows. Section II describes the psuedorange observation model. Section III describes the problem formulation, terrestrial SOP selection framework, and provides pseudocode for the proposed selection algorithm. Section IV presents simulation results comparing the two selection schemes' performance and computational complexity. Section V presents experimental results for an U.S. Air Force high-altitude aircraft using the proposed seleciton algorithm in an emulated GNSS-denied environment. Section VI contains concluding remarks.

II. PSEUDORANGE OBSERVATION MODEL

The pseudorange observation made by the receiver on the i-th SOP tower is modeled as

$$z_{s_i}(k) = \underbrace{\left\|\boldsymbol{r}_r(k) - \boldsymbol{r}_{s_i}\right\|_2 + c\delta t_i(k)}_{h_i[\boldsymbol{x}(k)]} + v_{s_i}(k), \quad i = 1, \cdots, M, \tag{1}$$

where M is the total number of SOPs, $\boldsymbol{r}_r$ is the aerial vehicle-mounted receiver's 3–D position state vector, $\boldsymbol{r}_{s_i}$ is the SOP's 3–D position vector, c is the speed of light, δt_i is the difference between the receiver's and SOP's clock biases, and v_{s_i} is the measurement noise, which is modeled as a zero-mean white Gaussian sequence with variance $\sigma^2_{s_i}$. It is assumed that the measurement noise is independent across the different terrestrial SOP towers. It is assumed that the SOP tower's position are known *a priori*. Furthermore, due to the poor geometric diversity of terrestrial SOPs in the vertical direction (which leads to large vertical dilution of precision (VDOP) if the aerial vehicle would exclusively rely on SOPs for 3–D navigation), it is assumed that the aerial vehicle is equipped with an altimeter to determine its altitude. As such, in what follows, the formulation will only consider the planar aerial vehicle states.

III. TERRESTRIAL SOP SELECTION FRAMEWORK

This section formulates terrestrial SOP selection problem. Next, it proposes the OGS algorithm for SOP selection, which is sub-optimal, yet computationally efficient.

1. Problem Formulation

Consider an aerial vehicle with knowledge of its initial states navigating in an environment containing an abundant number of terrestrial SOPs with *known* transmitter locations, but *unknown* clock error states. The aerial vehicle looses access to GNSS signals and is tasked with navigating by exploiting signals from the terrestrial SOPs. The aerial vehicle is assumed to be equipped with an on-board receiver capable of extracting pseudorange observations, modeled as (1), from the ambient SOPs' signals. The aerial vehicle fuses these observations through an estimator (e.g., EKF) to estimate the state vector $\boldsymbol{x}$ containing the aerial vehicle-mounted receiver's states and the clock error states between the receiver and the M SOPs. Due to size, weight, power, and cost (SWaP-C) constraints, the aerial vehicle-mounted receiver is constrained to using a subset ($K < M$) of the total number of terrestrial SOPs. This prompts the question of what is the "best" subset of SOPs to use? Fig. 1 illustrates a real-world environment in which this problem was encountered in Southern California, USA, where the white pins denote $M = 57$ cellular SOPs, which the aerial vehicle-mounted receiver was simultaneously tracking as it traveled along the green trajectory.

The transmitter selection problem can be cast as the following optimization problem

$$\begin{aligned} \underset{S}{\text{minimize}} \quad & \mathcal{J}\left[S\right] \\ \text{subject to} \quad & \boldsymbol{z}(k) = \boldsymbol{h}[\boldsymbol{x}(k)] \\ & n(S) = K, \end{aligned}$$

where $\mathcal{J}(\cdot)$ denotes a desired cost function (e.g., GDOP, A-optimality, E-optimality, etc.) [41,42], S is the set of selected SOPs, and $n(\cdot)$ denotes the cardinality of the set (i.e., number of elements in the set). This optimization problem is computationally involved to solve in real-time due to the integer constraints. Instead of directly solving the above optimization problem, the OGS algorithm is proposed, which is discussed next.

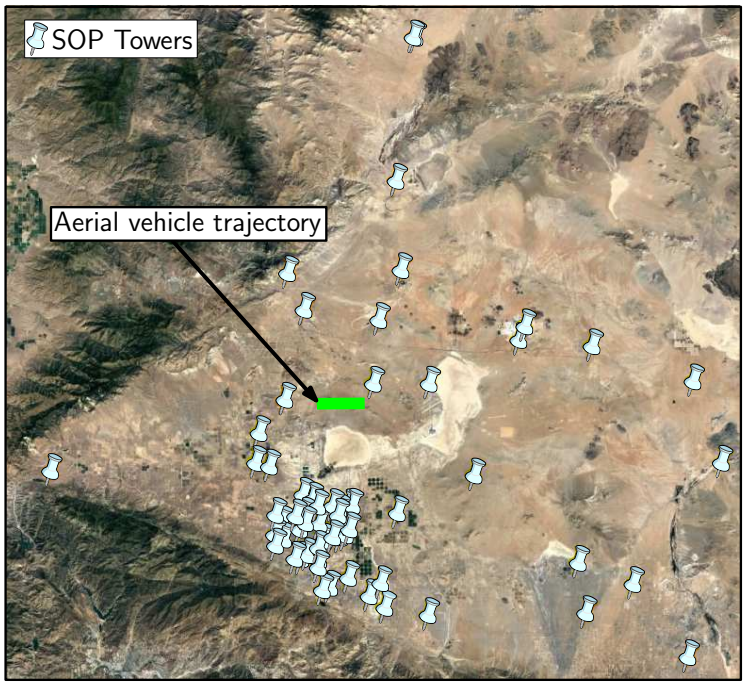

Figure 1: Problem motivation. Terrestrial SOP towers (white) in the environment along with the aerial vehicle's trajectory (green). Using all 57 SOP towers to navigate the aerial vehicle would violate SWaP-C constraints. As such, it is desired to choose the "best" subset of SOPs to use to navigate the aerial vehicle.

2. Fisher Information Matrix-Based Approach

The proposed OGS algorithm aims to select the transmitters yielding the most informative observations. This motivates adopting an FIM-based approach to construct the selection algorithm's cost function. The FIM is given as [43]

$$\mathbf{I}(\boldsymbol{x}) = \mathbb{E}\left[\left(\frac{\partial \ln p(\boldsymbol{z}|\boldsymbol{x})}{\partial \boldsymbol{x}}\right)\left(\frac{\partial \ln p(\boldsymbol{z}|\boldsymbol{\theta})}{\partial \boldsymbol{x}}\right)^{\mathsf{T}}\right], \tag{2}$$

where $p(\boldsymbol{z}|\boldsymbol{x})$ is the likelihood function of the measurements $\boldsymbol{z}$ parameterized by the states $\boldsymbol{x}$. Since the pseudrorange observation model (1) is assumed to have additive Gaussian noise, and the observations $\{z_{s_i}\}_{i=1}^{M}$ are assumed to be independent, the FIM associated with the i-th SOP tower simplifies to [44]

$$\mathbf{I}_i(\boldsymbol{x}) = \frac{1}{\sigma_{s_i}^2}\left(\frac{\partial h_i(\boldsymbol{x})}{\partial \boldsymbol{x}}\right)\left(\frac{\partial h_i(\boldsymbol{x})}{\partial \boldsymbol{x}}\right)^{\mathsf{T}}, \quad i = 1, \ldots, M. \tag{3}$$

This simplified FIM form provides the information content associated with the i-th observation, which is similar to the notion of information matrix associated with observations (IMAO) discussed in the robotics literature [45].

The additive property of information from different sources will be utilized in the OGS algorithm [46]. Denoting the (prior) information content associated with a subset of SOPs as $\mathbf{I}_{\text{prior}}(\boldsymbol{x})$ and the information associated with the i-th SOP as $\mathbf{I}_i(\boldsymbol{x})$, then the (posterior) information content associated with updating the SOP subset to include the i-th SOP is essentially $\mathbf{I}_{\text{posterior},i}(\boldsymbol{x}) = \mathbf{I}_{\text{prior}}(\boldsymbol{x}) + \mathbf{I}_i(\boldsymbol{x})$.

3. Transmitter Selection Algorithm

The proposed OGS algorithm is based on selecting the SOP subset that would minimize the aerial vehicle-mounted receiver's position error uncertainty. To this end, the information content associated with the receiver's position states will be maximized. The proposed OGS algorithm employs the EKF described in [47] to compute the FIMs, and the upper 2×2 block corresponding to the position states $\mathbf{I}_{\boldsymbol{r}_r}$ is used in the cost function evaluation. The cost function $\mathcal{J}$ will be chosen as the A-optimality criterion [48]: the trace of the posterior estimation error covariance (equivalently, the trace of the inverse of the FIM), namely

$$\mathcal{J}[S] \triangleq \text{tr}\left[\sum_{S} \mathbf{I}_{\boldsymbol{r}_r,i}\right]^{-1}, \tag{4}$$

It is worth noting that the equivalent Fisher Information Matrix (EFIM) [49, 50], which considers the information associated with the receiver's position states and non-position states, could also be employed.

The OGS proceeds as follows. First, an exhaustive search is performed to select the two SOPs containing the largest information content $\mathbf{I}_i(\boldsymbol{x})$, according to the A-optimality criterion. This exhaustive search is necessary to ensure that the system is observable before implementing the OGS strategy. In [47], it was shown that at least two SOPs with known locations are necessary to guarantee observability. Next, the information associated with each of the remaining SOPs $\mathbf{I}_i(\boldsymbol{x})$ (i.e., excluding the two already selected) is calculated, the one with the highest information (as evaluated by the A-optimality criterion) is added to the selection subset, and the posterior FIM is updated accordingly. This process of evaluating the information content from the remaining SOPs continues until the selection subset contains the desired number of SOPs. Algorithm 1 details the proposed OGS steps.

IV. SIMULATION RESULTS

This section presents simulation results to analyze the performance and computational cost of the proposed OGS algorithm versus that of the optimal selection algorithm (obtained by exhaustive search).

Algorithm 1 Opportunistic greedy selection algorithm

Input: $K,\ \mathbf{P}_{\boldsymbol{r}_r}(0|0),\ \{\mathbf{I}_{\boldsymbol{r}_r,i}\}_{i=1}^{M},\ \boldsymbol{x}_{\text{sop}} = \{1,\ldots,M\}$
Output: SOP indices contained in the selection subset S
1: Initialize an empty set $S = \phi$
2: Define the prior FIM as $\mathbf{I}_{\text{prior}} = [\mathbf{P}_{\boldsymbol{r}_r}(0|0)]^{-1}$
3: Perform an exhaustive search for the initial two transmitters
4: Choose the two transmitters which minimize

$$j_1^*, j_2^* = \underset{j_1,j_2}{\text{argmin}}\ \text{tr}\left(\left[\mathbf{I}_{\text{prior}} + \sum_{\ell=1}^{2}\mathbf{I}_{\boldsymbol{r}_r,j_\ell}\right]^{-1}\right),\ \forall j_1, j_2 = 1,\ldots,M;\ j_1 \neq j_2$$

5: Add the selected transmitters' indices to subset as $S \cup j_1^* \cup j_2^*$
6: Delete selected transmitter from original set as $\boldsymbol{x}_{\text{sop}} = \boldsymbol{x}_{\text{sop}} \setminus \{j_1^*, j_2^*\}$
7: Update the prior FIM with the selected SOPs

$$\mathbf{I}_{\text{prior}} = \mathbf{I}_{\text{prior}} + \mathbf{I}_{\boldsymbol{r}_r,j_1^*} + \mathbf{I}_{\boldsymbol{r}_r,j_2^*}$$

8: **for** α = 3 : K **do**
9: Compute the posterior FIM for all transmitters, excluding those in S

$$\mathbf{I}_{\text{posterior},i} = \mathbf{I}_{\text{prior}} + \mathbf{I}_{\boldsymbol{r}_r,i}, \quad \forall i = 1,\ldots,M \setminus \{S\}$$

10: Choose the transmitter which minimizes the receiver's average position uncertainty (A-optimality)

$$i^* = \underset{i}{\text{argmin}}\ \text{tr}\left[\mathbf{I}_{\text{posterior},i}^{-1}\right]$$

11: Add the selected transmitter index to subset as $S \cup i^*$
12: Delete selected transmitter from original set as $\boldsymbol{x}_{\text{sop}} = \boldsymbol{x}_{\text{sop}} \setminus \{i^*\}$
13: Update the prior FIM with the selected SOP

$$\mathbf{I}_{\text{prior}} = \mathbf{I}_{\text{prior}} + \mathbf{I}_{\boldsymbol{r}_r,i^*}$$

14: **end for**
15: **return** S

1. Simulation Settings

The simulated environment consisted of $M = 30$ terrestrial SOP towers with known locations. The aerial vehicle was assumed to move with velocity random walk dynamics, while making pseudorange observations to these SOPs, which are fused through an EKF as described in [47]. It was assumed that the aerial vehicle had a known vertical position, which reduces the aerial vehicle's position states estimated in the EKF to the planar states. The aerial vehicle had initial access to GNSS signals, leading to knowledge of its initial states (position, velocity, clock bias, and clock drift), after which the aerial vehicle looses access to GNSS. During the period of GNSS availability, the vehicle chooses the best $K < M$ SOPs to be used to navigate with, once GNSS signals are cut off. The aerial vehicle's process noise spectral density was assumed to be $\tilde{q}_x = \tilde{q}_y = 0.1\ \text{m}^2/\text{s}^3$ and the sampling period was set to $T = 0.01$ s. The aerial vehicle-mounted receiver's clock was assumed to be a typical oven-controlled crystal oscillator (OCXO) with $\{h_{0,r},\ h_{-2,r}\} = \left\{8.0 \times 10^{-20}\ \text{s},\ 4.0 \times 10^{-23}\ \text{s}^{-1}\right\}$, while the SOPs' clocks were assumed to be equipped with a high-quality OCXO with $\{h_{0,s_i},\ h_{-2,s_i}\} = \left\{2.6 \times 10^{-22}\ \text{s},\ 4.0 \times 10^{-26}\ \text{s}^{-1}\right\}$.

The EKF initial state estimate $\hat{\boldsymbol{x}}(0|0)$ was generated from $\hat{\boldsymbol{x}}(0|0) \sim \mathcal{N}[\boldsymbol{x}(0|0),\ \mathbf{P}(0|0)]$, where $\mathbf{P}(0|0)$ is the EKF initial estimation error covariance. The aerial vehicle-mounted receiver's initial state vector was assumed to be $\boldsymbol{x}_r(0|0) = [0,\ 50,\ 15,\ 0,\ 10,\ 1]^\mathsf{T}$ and the initial clock error state vector for all M SOPs was assumed to be $\boldsymbol{x}_{\text{clk}}(0|0) = [1,\ 0.1]^\mathsf{T}$. The measurement noise variance was assumed to be $\sigma_{s_i}^2 = 25\ \text{m}^2, \forall i = 1,\ \ldots,\ M$. The initial estimation error covariance matrices of the receiver and the SOPs' clock error states were chosen to be $\mathbf{P}_r(0|0) = \text{diag}[25,\ 25,\ 9,\ 9]$ and $\mathbf{P}_{s_i}(0|0) = \text{diag}[30 \times 10^3,\ 0.3 \times 10^3]$.

2. Generating Terrestrial SOP Locations

The cellular SOP network was modeled as a binomial point process (BPP), where the horizontal positions of the M SOPs are independently and uniformly distributed over an annular region centered at the aerial vehicle's current position O, i.e., $\mathbb{B}_O\left(d_{\min}, d_{\max}\right) = \pi(d_{\max}^2 - d_{\min}^2)$ [51], where $d_{\max}$ is the maximum distance for which ranging signals can be detected by the receiver and $d_{\min}$ is the minimum distance required for the far-field assumption to hold (See Fig. 2(a) for $M = 30$). The location of the i-th SOP is represented in terms of its range R_i and its aerial vehicle-to-SOP bearing angle θ_i by $(R_i\cos(\theta_i),\ R_i\sin(\theta_i))$, as shown in Fig. 2(b).

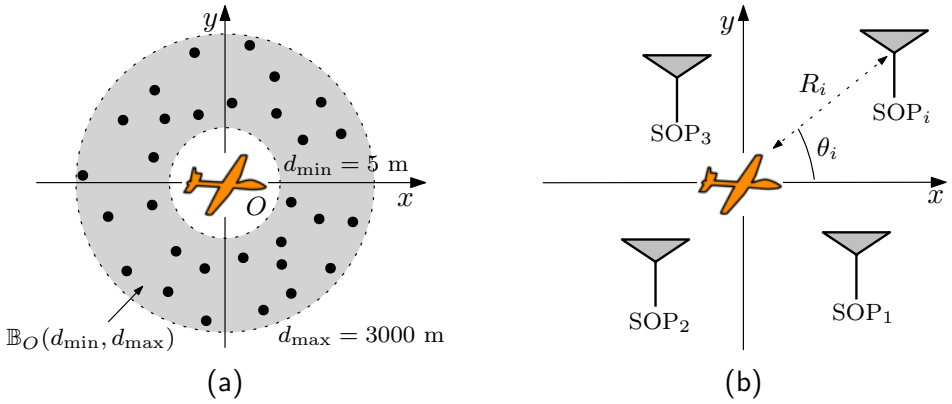

Figure 2: (a) BPP realization with $M = 30$ SOPs. (b) Parameterization of the i-th SOP's position.

3. Numerical Results

Two selection algorithms were considered. The first algorithm was to perform an exhaustive M choose K selection, i.e., $\binom{M}{K} = \frac{M!}{(M-K)!K!}$, to provide the optimal transmitter selection by calculating the global optimum solution to the transmitter selection optimization problem. Note that this algorithm is extremely computationally extensive. The second algorithm is the the proposed OGS algorithm, which provides a sub-optimal, yet computationally efficient, transmitter selection.

The environment shown in Fig. 2 comprising $M = 30$ terrestrial SOPs is simulated and it is assumed that the aerial vehicle wants to select $K = 15$ SOPs.

The solutions resulting from the algorithms, M choose K and proposed OGS, are displayed in Fig. 3. Note that the both algorithm yielded comparable selection. The A-optimality, E-optimality, and GDOP performance metrics are utilized to quantify the estimation performance of the selected SOPs. The A-optimality measure corresponds to the average variance of the state estimates and the E-optimality measure corresponds to the length of the largest axis of the uncertainty covariance ellipsoid [41]. Table 1 presents the performance values attained for the two algorithms.

As expected, the M choose K selection algorithm yielded the best performance metric values for the A-optimality criterion. It also yielded the best performance for the E-optimality and the the GDOP criteria. Nevertheless, the OGS algorithm was not too far behind. Moreover, the OGS algorithm was quite close to the optimal cost function evaluation. Specifically, the M choose K global minimum was found to be $\mathcal{J}\left[\mathbf{I}_{\boldsymbol{r}_r}(S^*)\right] = 49.6915$ whereas the OGS local minimum was found to be $\mathcal{J}\left[\mathbf{I}_{\boldsymbol{r}_r}(S)\right] = 49.7065$. It is important to note that the optimal M choose K selection came at the price of computational cost (i.e., run-time). The M choose K algorithm took 10 hours to run on a computer with processor base frequency @ 3.00 GHz and CPU with 8-cores, 8-threads; whereas the OGS algorithm took only 7.5 millisecond to run.

Table 1: Performance Metric Comparison for Selection Algorithms

	$\text{tr}[\mathbf{I}_{\boldsymbol{r}_r}^{-1}(S)]$	$\lambda_{\max}[\mathbf{I}_{\boldsymbol{r}_r}^{-1}(S)]$	GDOP	Time to Run
M Choose K	49.6915	24.8462	0.577	10.03 hours
OGS	49.7065	24.8620	0.592	7.50 milliseconds

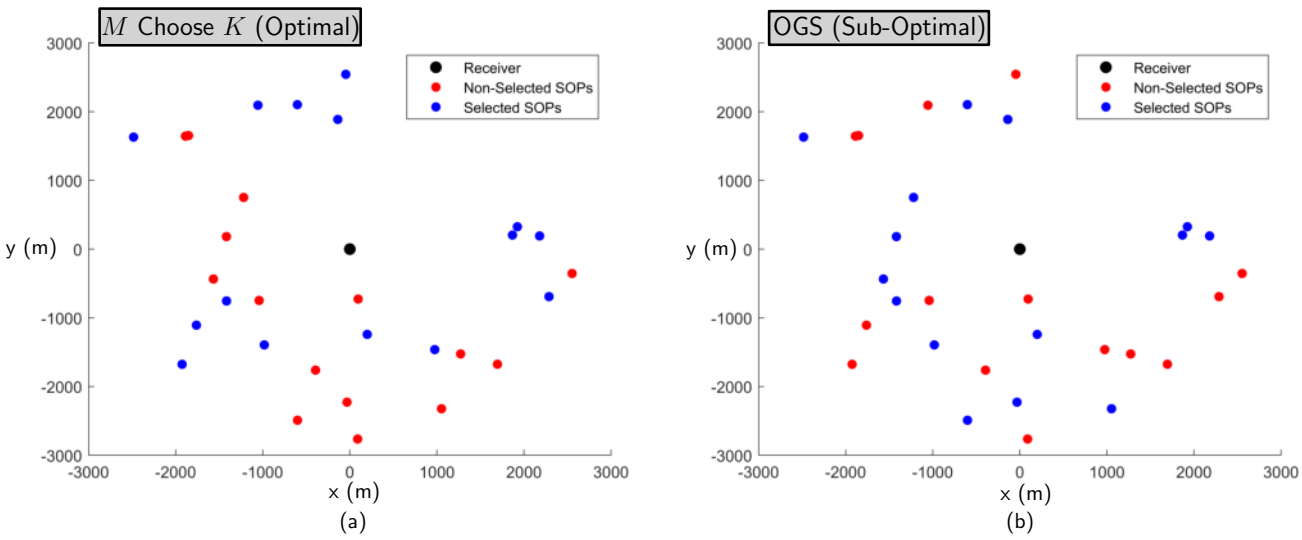

Figure 3: Selection algorithm comparison. (a) M choose K. (b) Opportunistic Greedy Selection

4. Computational Cost

The computational cost of using the optimal M choose K algorithm grows exponentially [52], while it grows linearly for the OGS algorithm. Fig. 4 compares the time to run each algorithm.

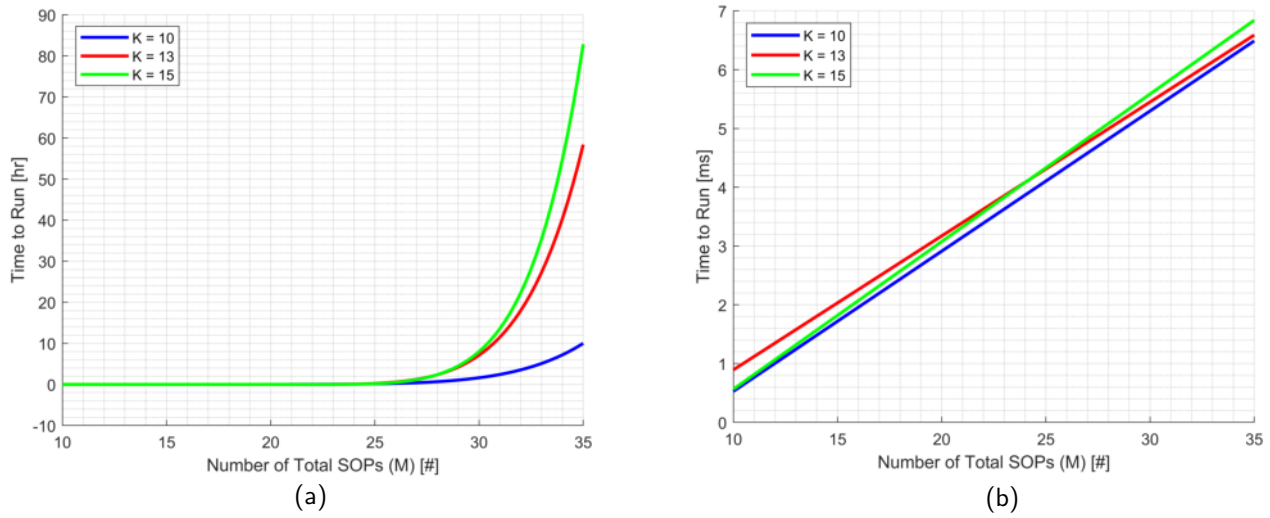

Figure 4: Time to run of selection algorithms: (a) M choose K. (b) OGS.

V. EXPERIMENTAL RESULTS

This section demonstrates the efficacy of the proposed OGS algorithm in selecting a "manageable" subset of terrestrial SOP pseudoranges to navigate an aircraft in a real-world environment.

In March 2020, a joint effort between the Autonomous Systems Perception, Intelligence, and Navigation Laboratory (ASPIN) and Edwards Air Force Base (AFB), California, U.S.A. led to week-long flights in a mission called "SNIFFER: Signals of opportunity for Navigation In Frequency-Forbidden EnviRonments." The flights took place on a Beechcraft C12 Huron, a fixed-wing U.S. Air Force aircraft, flown by members of the USAF Test Pilot School (TPS).

The C-12 aircraft was equipped with a quad-channel universal software radio peripheral (USRP)-2955, three consumer-grade

800/1900 MHz Laird cellular antennas, GPS antenna, a solid-state drive for data storage, and a laptop computer running ASPIN Laboratory's software-defined radio (SDR), called MATRIX: Multichannel Adaptive TRansceiver Information eXtractor, for real-time monitoring of the cellular signals [16,53,54]. Furthermore, the equipment necessary for the experiment was assembled at the ASPIN Laboratory on a special rack provided by the U.S. Air Force and was mounted on the C-12 aircraft. MATRIX produces the navigation observables, i.e., Doppler frequency, carrier phase, and pseudorange. The experimental hardware setup is shown in Fig. 5.

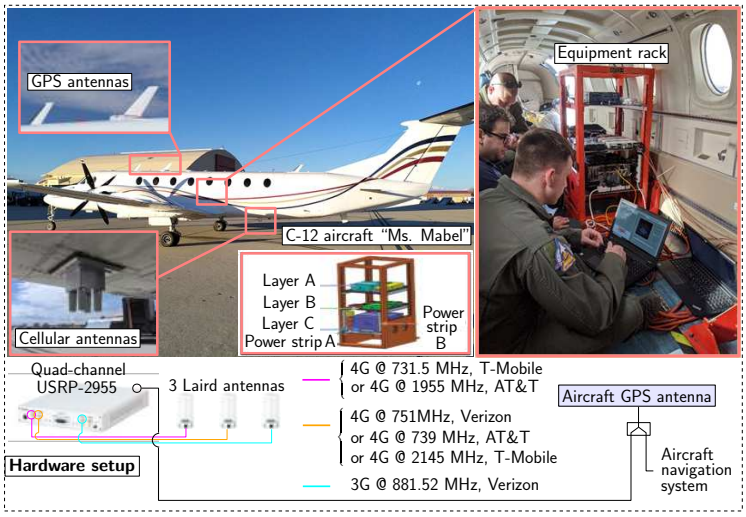

Figure 5: Hardware setup equipped to the C-12 aircraft.

The C-12 aircraft fused both pseudorange observations and altimeter measurements in an EKF-based navigation filter. The environment was comprised of $M = 57$ terrestrial cellular SOPs, where the aircraft was tasked with selecting a subset of $K = 15$ with which to navigate after GNSS cutoff. The aircraft's state vector was initialized with $[\hat{\boldsymbol{r}}_r(0|0)^\mathsf{T},\ \dot{\hat{\boldsymbol{r}}}_r(0|0)^\mathsf{T}]^\mathsf{T} = [-8.97,\ 6.86,\ 1982.53,\ 85.21,\ -11.53,\ 0.28]^\mathsf{T}$, whereas the modified clock error states of each SOP was initialized using the pseudorange observations from the initial two time epochs. Specifically, the clock bias was initialized as $c\delta t_i(0|0) = z_{s_i}(0) - \|\boldsymbol{r}_r(0) - \boldsymbol{r}_{s_i}\|_2$ and the clock drift was initialized as $c\dot{\delta} t_i(0|0) = \frac{1}{T}[z_{s_i}(1) - z_{s_i}(0) - \|\boldsymbol{r}_r(1) - \boldsymbol{r}_{s_i}\|_2 + \|\boldsymbol{r}_r(0) - \boldsymbol{r}_{s_i}\|_2]$, respectively.

Therefore, the initial state vector was constructed as $\hat{\boldsymbol{x}}(0|0) = [\hat{\boldsymbol{r}}_r(0|0)^\mathsf{T},\ \dot{\hat{\boldsymbol{r}}}_r(0|0)^\mathsf{T},\ c\hat{\delta t}_1(0|0),\ c\dot{\hat{\delta t}}_1(0|0), \ldots,\ c\hat{\delta t}_K(0|0),\ c\dot{\hat{\delta t}}_K(0|0)]^\mathsf{T}$ with a corresponding initial estimation error covariance defined as $\mathbf{P}(0|0) = \text{diag}[100{\cdot}\mathbf{I}_{3\times3},\ 10{\cdot}\mathbf{I}_{3\times3},\ 10^8,\ 10, \ldots,\ 10^8,\ 10]^\mathsf{T}$. The receiver's clock covariance $\mathbf{Q}_{\text{clk},r}$ was set to correspond to a typical OCXO with $h_{0,r} = 9.4 \times 10^{-20}$ s and $h_{-2,r} = 3.8 \times 10^{-21}$ s^{-1}. The SOPs' clock covariance $\mathbf{Q}_{\text{clk},s_i}$ was set to correspond to a typical OCXO with $h_{0,s_i} = 8.0 \times 10^{-20}$ s and $h_{-2,s_i} = 4.0 \times 10^{-23}$ s^{-1}. Furthermore, the aircraft's dynamics were assumed to evolve according to a velocity random walk model [55], with $\tilde{q}_x = \tilde{q}_y = 5$ m^2/s^3 and $\tilde{q}_z = 0.1$ m^2/s^3 being the x, y, and z continuous-time acceleration noise spectra and the sampling time $T = 0.01$ s. The measurement covariance $\mathbf{R}$ was assumed to be time-varying and proportional to the inverse of the carrier-to-noise ratio at each time step.

The OGS algorithm was implemented to choose a selection subset S consisting of $K = 15$ SOPs after access to GNSS signals was cut off. The selected SOPs from the OGS algorithm are denoted by the red pins whereas the non-selected SOPs are denoted by white pins in Fig. 6(a). The aircraft finished navigated along the green trajectory in Fig. 6(a) for 9.39 km in 105 s, by utilizing the selected SOPs. The aircraft's position and velocity root mean square error (RMSEs) were found to be 11.45 m and 0.80 m/s, respectively. The OGS algorithm ran in 25.5 ms and the navigation filter ran in 18.33 s, which makes this selection scheme and navigation framework readily implementable in real-time. It should be noted, the optimal solution (i.e., global minimum) for SOP selection is impractical to compute using the M choose K algorithm due to formidable time it would take to run. In light of this, 10,000 Monte Carlo runs were performed in an attempt to capture the range of best-to-worst selections. The randomized parameter for the MC runs was the selection subset S.

Table 2 summarizes the navigation performance with the proposed OGS selection versus the range of obtained performance (i.e., [minimum, maximum]) with the MC selection. Table 3 shows the A-optimality cost function, E-optimality measure, and GDOP performance metrics resulting from the OGS algorithm.

Fig. 6(b) plots the histogram of the position and velocity RMSEs from the MC runs. These figures provides insight into the error distribution of the aircraft's navigation solution for the ensemble of randomized realizations. Notice, the OGS algorithm's position RMSE value is placed in the left-most histogram bin which, implying that the OGS's navigation solution is close to the navigation solution obtained when using the best MC realization.

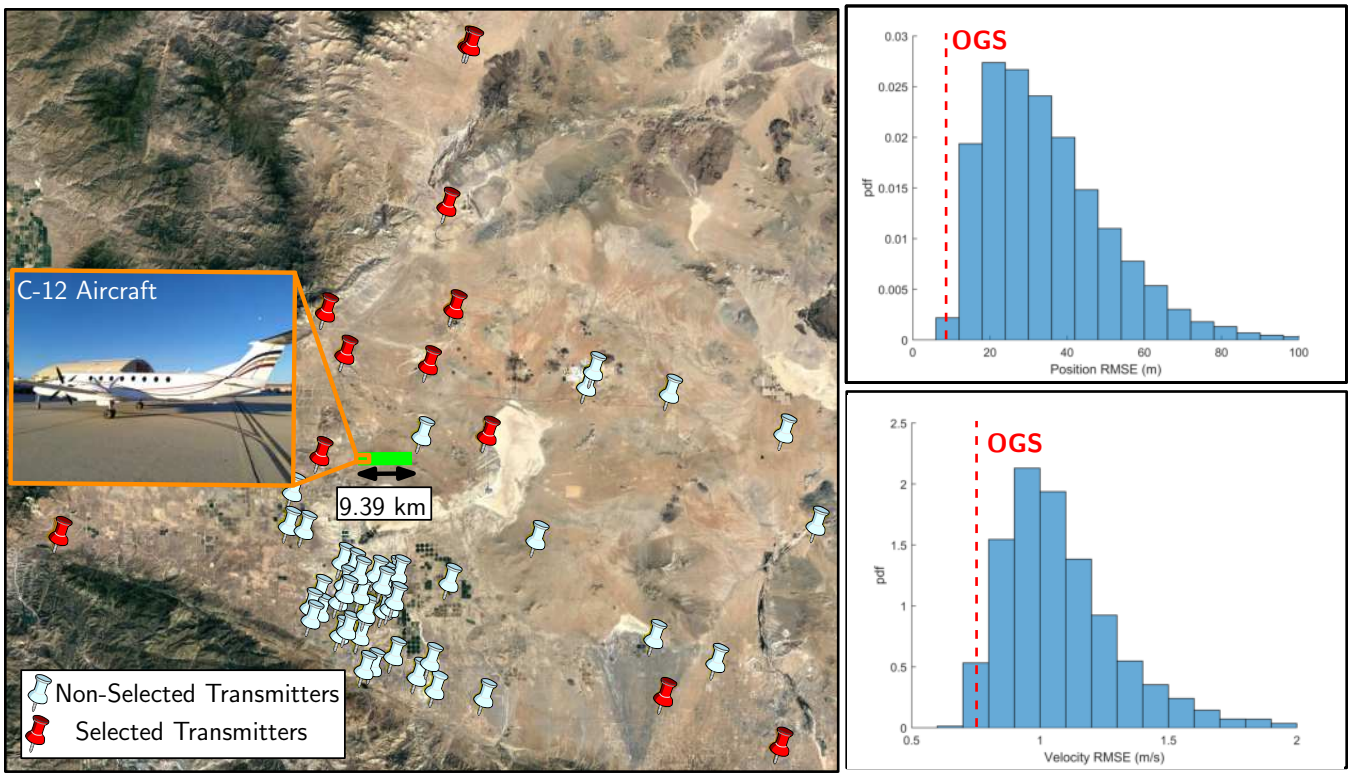

(a) (b)

Figure 6: (a) Experimental layout and results using the proposed OGS algorithm for transmitter selection during the aircraft's flight. (b) Histogram of the position and velocity RMSEs due to 10,000 different randomized transmitter selections versus the proposed OGS algorithm's RMSEs, marked with a red dashed line.

Table 2: Performance of Navigation Solution

Selection Type	Pos. RMSE [m]	Vel. RMSE [m/s]	Max Pos. Error [m]	Max Vel. Error [m/s]
Opportunistic Greedy Selection (OGS)	11.4513	0.8026	26.8908	4.3277
10,000 MC Simulations	[8.0739, 157.4984]	[0.6587, 2.7495]	[11.6528, 327.6256]	[4.3112, 10.1685]

Table 3: Performance Metrics for Opportunistic Greedy Selection

	$\mathrm{tr}\left[\mathbf{I}_{\boldsymbol{r}_r}^{-1}(S)\right]$	$\lambda_{\max}\left[\mathbf{I}_{\boldsymbol{r}_r}^{-1}(S)\right]$	GDOP	Time to Run
Opportunistic Greedy Selection (OGS)	200.99	100.00	0.62	25.50 ms

VI. CONCLUSION

This paper presented a computationally efficient algorithm to choose the most informative subset of terrestrial SOPs to use for navigation purposes. The proposed OGS algorithm is formulated by exploiting the additive, iterative properties of the FIM, to minimize the aerial vehicle's average position error variance. Numerical simulations are presented showing that the proposed OGS algorithm performs comparably with the optimal M choose K selection algorithm, but executes in a small fraction of

the time. Experimental results are presented for a U.S. Air Force high-altitude aircraft navigating without GNSS signals in an environment comprising $M = 57$ cellular terrestrial SOPs for 9.39 km in 105 s. It is shown that upon choosing $K = 15$ SOPs according to the proposed OGS algorithm, the position and velocity root mean square errors (RMSEs) were 11.45 m and 0.80 m/s, respectively. Monte Carlo results are presented arguing that the results achieved from the proposed OGS algorithm are very close to what the global optimal selection algorithm would yield.

ACKNOWLEDGMENTS

The authors would like to thank Zeinab Shadram for helpful discussions and Ali for help with data processing. The authors would also like to thank Edwards Air Force Base (AFB) and Holloman AFB for inviting the ASPIN Laboratory to conduct experiments on U.S. Air Force aircraft in the "SNIFFER: Signals of opportunity for Navigation In Frequency-Forbidden EnviRonments" flight campaign. The authors would like to thank Joshua Morales, Kimia Shamaei, Mahdi Maaref, Kyle Semelka, MyLinh Nguyen, and Trier Mortlock for their help with preparing for data collection. DISTRIBUTION STATEMENT A. Approved for public release; Distribution is unlimited. 412TW-PA-20146.

This work was supported in part by the the National Science Foundation (NSF) under Grant 1929571 and in part by the Office of Naval Research (ONR) under Grant N00014-19-1-2613. This work was also supported in part by the Laboratory Directed Research and Development program at Sandia National Laboratories, a multimission laboratory managed and operated by National Technology and Engineering Solutions of Sandia LLC, a wholly owned subsidiary of Honeywell International Inc. for the U.S. Department of Energy's National Nuclear Security Administration under contract DE-NA0003525. This paper describes objective technical results and analysis. Any subjective views or opinions that might be expressed in the paper do not necessarily represent the views of the U.S. Department of Energy or the United States Government.

REFERENCES

[1] R. Sabatini, A. Roy, E. Blasch, K. Kramer, , G. Fasano, I. Majid, O. Crespillo, D. Brown, and R. Ogan, "Avionics systems panel research and innovation perspectives," *IEEE Aerospace and Electronic Systems Magazine*, vol. 35, no. 12, pp. 58–72, December 2020.

[2] R. Ioannides, T. Pany, and G. Gibbons, "Known vulnerabilities of global navigation satellite systems, status, and potential mitigation techniques," *Proceedings of the IEEE*, vol. 104, no. 6, pp. 1174–1194, February 2016.

[3] EUROCONTROL, Aviation Intelligence Unit, "Does radio frequency interference to satellite navigation pose an increasing threat to network efficiency, cost-effectiveness and ultimately safety?" Tech. Rep.

[4] International Civil Aviation Organization (ICAO), "An urgent need to address harmful interferences to GNSS," https://www.iata.org/contentassets/e45e5219cc8c4277a0e80562590793da/address-harmful-interferences-gnss.pdf, Tech. Rep., May 2019.

[5] J. Raquet *et al.*, "Position, navigation, and timing technologies in the 21st century," J. Morton, F. van Diggelen, J. Spilker, Jr., and B. Parkinson, Eds. Wiley-IEEE, 2021, vol. 2, Part D: Position, Navigation, and Timing Using Radio Signals-of-Opportunity, ch. 35–43, pp. 1115–1412.

[6] N. Souli, P. Kolios, and G. Ellinas, "Online relative positioning of autonomous vehicles using signals of opportunity," *IEEE Transactions on Intelligent Vehicles*, pp. 1–1, 2021.

[7] J. McEllroy, "Navigation using signals of opportunity in the AM transmission band," Master's thesis, Air Force Institute of Technology, Wright-Patterson Air Force Base, Ohio, USA, 2006.

[8] X. Chen, Q. Wei, F. Wang, Z. Jun, S. Wu, and A. Men, "Super-resolution time of arrival estimation for a symbiotic FM radio data system," *IEEE Transactions on Broadcasting*, vol. 66, no. 4, pp. 847–856, December 2020.

[9] J. del Peral-Rosado, R. Raulefs, J. Lopez-Salcedo, and G. Seco-Granados, "Survey of cellular mobile radio localization methods: from 1G to 5G," *IEEE Communications Surveys & Tutorials*, vol. 20, no. 2, pp. 1124–1148, 2018.

[10] J. Gante, L. Sousa, and G. Falcao, "Dethroning GPS: Low-power accurate 5G positioning systems using machine learning," *IEEE Journal on Emerging and Selected Topics in Circuits and Systems*, vol. 10, no. 2, pp. 240–252, June 2020.

[11] P. Wang and Y. Morton, "Multipath estimating delay lock loop for LTE signal TOA estimation in indoor and urban environments," *IEEE Transactions on Wireless Communications*, vol. 19, no. 8, pp. 5518–5530, 2020.

[12] J. Mortier, G. Pages, and J. Vila-Valls, "Robust TOA-based UAS navigation under model mismatch in GNSS-denied harsh environments," *Remote Sensing*, vol. 12, no. 18, pp. 2928–2947, September 2020.

[13] H. Dun, C. Tiberius, and G. Janssen, "Positioning in a multipath channel using OFDM signals with carrier phase tracking," *IEEE Access*, vol. 8, pp. 13 011–13 028, 2020.

[14] J. Khalife and Z. Kassas, "Opportunistic UAV navigation with carrier phase measurements from asynchronous cellular signals," *IEEE Transactions on Aerospace and Electronic Systems*, vol. 56, no. 4, pp. 3285–3301, August 2020.

[15] T. Kazaz, G. Janssen, J. Romme, and A. Van der Veen, "Delay estimation for ranging and localization using multiband channel state information," *IEEE Transactions on Wireless Communications*, pp. 1–16, September 2021.

[16] A. Abdallah and Z. Kassas, "UAV navigation with 5G carrier phase measurements," in *Proceedings of ION GNSS Conference*, September 2021, pp. 3294–3306.

[17] R. Faragher and R. Harle, "Towards an efficient, intelligent, opportunistic smartphone indoor positioning system," *NAVIGATION, Journal of the Institute of Navigation*, vol. 62, no. 1, pp. 55–72, 2015.

[18] Y. Zhuang, Y. Li, L. Qi, H. Lan, J. Yang, and N. El-Sheimy, "A two-filter integration of MEMS sensors and WiFi fingerprinting for indoor positioning," *IEEE Sensors Journal*, vol. 16, no. 13, pp. 5125–5126, 2016.

[19] C. Yang and A. Soloviev, "Mobile positioning with signals of opportunity in urban and urban canyon environments," in *Proceedings of IEEE/ION Position, Location, and Navigation Symposium*, April 2020, pp. 1043–1059.

[20] T. Hong, J. Sun, T. Jin, Y. Yi, and J. Qu, "Hybrid positioning with DTMB and LTE signals," in *Proceedings of International Wireless Communications and Mobile Computing*, July 2021, pp. 303–307.

[21] Y. Meng, L. Bian, L. Han, W. Lei, T. Yan, M. He, and X. Li, "A global navigation augmentation system based on LEO communication constellation," in *Proceedings of European Navigation Conference*, May 2019, pp. 65–71.

[22] R. Landry, A. Nguyen, H. Rasaee, A. Amrhar, X. Fang, and H. Benzerrouk, "Iridium Next LEO satellites as an alternative PNT in GNSS denied environments–part 1," *Inside GNSS Magazine*, vol. 14, no. 3, pp. 56–64., May 2019.

[23] Z. Kassas, J. Morales, and J. Khalife, "New-age satellite-based navigation – STAN: simultaneous tracking and navigation with LEO satellite signals," *Inside GNSS Magazine*, vol. 14, no. 4, pp. 56–65, 2019.

[24] F. Farhangian, H. Benzerrouk, and R. Landry, "Opportunistic in-flight INS alignment using LEO satellites and a rotatory IMU platform," *Aerospace*, vol. 8, no. 10, pp. 280–281, 2021.

[25] Z. Kassas, M. Neinavaie, J. Khalife, N. Khairallah, J. Haidar-Ahmad, S. Kozhaya, and Z. Shadram, "Enter LEO on the GNSS stage: Navigation with Starlink satellites," *Inside GNSS Magazine*, vol. 16, no. 6, pp. 42–51, 2021.

[26] J. Morales and Z. Kassas, "Tightly-coupled inertial navigation system with signals of opportunity aiding," *IEEE Transactions on Aerospace and Electronic Systems*, vol. 57, no. 3, pp. 1930–1948, 2021.

[27] C. Cadena, L. Carlone, H. Carrillo, Y. Latif, D. Scaramuzza, J. Neira, I. Reid, and J. Leonard, "Past, present, and future of simultaneous localization and mapping: Toward the robust-perception age," *IEEE Transactions on robotics*, vol. 32, no. 6, pp. 1309–1332, 2016.

[28] V. Kekatos and G. Giannakis, "Selecting reliable sensors via convex optimization," in *Proceedings of IEEE International Workshop on Signal Processing Advances in Wireless Communications*, June 2010, pp. 1–5.

[29] S. Liu, S. Chepuri, M. Fardad, E. Masazade, G. Leus, and P. Varshney, "Sensor selection for estimation with correlated measurement noise," *IEEE Transactions on Signal Processing*, vol. 64, no. 13, pp. 3509–3522, July 2016.

[30] Z. D. G. W. X. Jin and X. Lou, "Nearly optimal sensor selection for TDOA-based source localization in wireless sensor networks," *IEEE Transactions on Vehicular Technology*, vol. 69, no. 10, pp. 12 031–12 042, July 2020.

[31] J. Morales and Z. Kassas, "Optimal collaborative mapping of terrestrial transmitters: receiver placement and performance characterization," *IEEE Transactions on Aerospace and Electronic Systems*, vol. 54, no. 2, pp. 992–1007, April 2018.

[32] V. Cerone, S. Fosson, and D. Regruto, "A non-convex adaptive regularization approach to binary optimization," in *Proceedings of IEEE Conference on Decision and Control*, February 2021, pp. 3844–3849.

[33] M. Shamaiah, S. Banerjee, and H. Vikalo, "Greedy sensor selection: Leveraging submodularity," in *Proceedings of IEEE Conference on Decision and Control (CDC)*, 2010, pp. 2572–2577.

[34] A. Hashemi, M. Ghasemi, H. Vikalo, and U. Topcu, "Randomized greedy sensor selection: Leveraging weak submodularity," *IEEE Transactions on Automatic Control*, vol. 66, no. 1, pp. 199–212, January 2021.

[35] L. Kaplan, "Local node selection for localization in a distributed sensor network," *IEEE Transactions on Aerospace and Electronic Systems*, vol. 42, no. 1, pp. 136–146, March 2006.

[36] L. Zuo, R. Niu, and P. Varshney, "A sensor selection approach for target tracking in sensor networks with quantized measurements," in *Proceedings of IEEE International Conference on Acoustics, Speech, and Signal Processing*, April 2008, pp. 2521–2524.

[37] X. Shen and P. Varshney, "Sensor selection based on generalized information gain for target tracking in large sensor networks," *IEEE Transactions on Signal Processing*, vol. 62, no. 2, pp. 363–375, January 2014.

[38] F. Wang, X. Bai, B. Guo, and C. Liu, "Dynamic clustering in wireless sensor network for target tracking based on the fisher information of modified kalman filter," in *Proceedings of IEEE International Conference of Systems and Informatics*, November 2016, pp. 696–700.

[39] M. Zhang and J. Zhang, "A fast satellite selection algorithm: Beyond four satellites," *IEEE Journal of Selected Topics in Signal Processing*, vol. 3, no. 5, pp. 740–747, October 2009.

[40] N. Blanco-Delgado and F. Nunes, "Satellite selection method for multi-constellation GNSS using convex geometry," *IEEE Transactions on Vehicular Technology*, vol. 59, no. 9, pp. 4289–4297, November 2010.

[41] D. Uciński, *Optimal Measurement Methods for Distributed Parameter System Identification*. CRC Press, 2005.

[42] N. Blanco-Delgado, F. Nunes, and G. Seco-Granados, "Relation between GDOP and the geometry of the satellite constellation," in *International Conference on Localization and GNSS*, June 2011, pp. 175–180.

[43] S. Kay, *Fundamentals of Statistical Signal Processing: Estimation Theory*. Prentice-Hall, Upper Saddle River, NJ, 1993, vol. I.

[44] S. Chepuri and G. Leus, "Sparsity-promoting sensor selection for non-linear measurement models," *IEEE Transactions on Signal Processing*, vol. 63, no. 3, pp. 684–698, February 2015.

[45] L. Perera and E. Nettleton, "On stochastically observable directions of the estimation theoretic SLAM state space," in *Proceedings of IEEE/RSJ International Conference on Intelligent Robots and Systems*, October 2010, pp. 4324–4331.

[46] G. Mutambara, *Decentralized Estimation and Control for Multisensor Systems*. CRC Press, 1998.

[47] A. Nguyen, Z. Shadram, and Z. Kassas, "A lower bound for the error covariance of radio SLAM with terrestrial signals of opportunity," in *Proceedings of ION GNSS Conference*, September 2021, pp. 2294–2306.

[48] Z. Kassas, A. Arapostathis, and T. Humphreys, "Greedy motion planning for simultaneous signal landscape mapping and receiver localization," *IEEE Journal of Selected Topics in Signal Processing*, vol. 9, no. 2, pp. 247–258, March 2015.

[49] Y. Shen and M. Win, "Fundamental limits of wideband localization–Part I: A general framework," *IEEE Transactions on Information Theory*, vol. 56, no. 10, pp. 4956–4980, October 2010.

[50] Y. Wang, Y. Wu, and Y. Shen, "Performance limits of cooperative localization using signals of opporunity in aray networks," in *Proceedings of IEEE International Conference on Communications*, May 2019, pp. 1–6.

[51] S. Aditya, H. Dhillon, A. Molisch, R. Buehrer, and H. Behairy, "Characterizing the impact of SNR heterogeneity on time-of-arrival-based localization outage probability," *IEEE Transactions on Wireless Communications*, vol. 18, no. 1, pp. 637–649, January 2019.

[52] S. Joshi and S. Boyd, "Sensor selection via convex optimization," *IEEE Transactions on Signal Processing*, vol. 57, no. 2, pp. 451–462, February 2009.

[53] J. Khalife, K. Shamaei, and Z. Kassas, "Navigation with cellular CDMA signals – part I: Signal modeling and software-defined receiver design," *IEEE Transactions on Signal Processing*, vol. 66, no. 8, pp. 2191–2203, April 2018.

[54] K. Shamaei and Z. Kassas, "LTE receiver design and multipath analysis for navigation in urban environments," *NAVIGATION, Journal of the Institute of Navigation*, vol. 65, no. 4, pp. 655–675, December 2018.

[55] X. Li and V. Jilkov, "Survey of maneuvering target tracking. Part I: Dynamic models," *IEEE Transactions on Aerospace and Electronic Systems*, vol. 39, no. 4, pp. 1333–1364, 2003.